PAPER

Check for updates

Optimization of drop-casting parameters for fabrication of n-type accumulation mode organic electrochemical transistors (OECTs) using gNDI-Br$_2$

Seongdae Kang, [ID] [a] Jiaxin Fan [ID] [b] and Manisha Gupta [ID] *[b]

Organic electrochemical transistors (OECTs) have received significant attention because of their unique operating mechanisms and diverse applications. We have reported the synthesis of an n-type naphthalene diimide (NDI)-based small-molecule OMIEC, gNDI-Br$_2$, which could be employed as the channel material for OECTs, and their fabrication parameters still need to be further examined. Here, we have explored the performance optimization of drop-cast gNDI-Br$_2$ OECTs by investigating various processing parameters that affect their functionality, including the solution concentration, number of drop-cast layers, and annealing temperature. Upon investigating different concentrations of the gNDI-Br$_2$ solution, we concluded that higher concentrations (>50 mg mL^{-1}) resulted in more than two-fold improved OECT transconductance ($g_m = 813.7 \pm 124.2$ μS for 100 mg mL^{-1}). By increasing the number of drop-cast gNDI-Br$_2$ layers, OECTs showed consistent maximum drain current ($I_{D,max}$) and an improvement in transconductance (g_m). Increasing the solution concentration and number of layers results in more densely packed gNDI-Br$_2$ molecules within the channel area, allowing enhanced electron transport and device performance. By increasing the thin film annealing temperature to 120 °C, a significant enhancement in device performance was achieved, with a more than five times increase in the normalized g_m (5.73 $\pm$ 0.87 mS cm^{-1}), which is likely due to enhanced molecular rearrangement at a higher processing temperature. Hence, this study provides valuable insights into the optimization of gNDI-Br$_2$ OECT performance through parameter exploration. Future work will focus on refining the fabrication techniques and material selection to further enhance device stability and functionality.

Introduction

The first report of organic electrochemical transistors (OECTs) by Wrighton *et al.*,[1] led to extensive research for the past few decades[2] for various applications, including circuits,[3] neuromorphics,[4,5] and biosensors.[6,7] OECTs have a unique operating mechanism compared to other organic thin-film transistors (OTFTs). OECTs are ion-permeable, which means that there is ion exchange between the channel and electrolyte when a gate potential (V_G) is applied, which changes the doping state and electrical conductivity of the entire channel material. This leads to volumetric conduction within the channel, and the electronic current is driven by the bias between the source and drain electrodes (V_D).[8] OECTs show high transconductance (g_m) at low operation voltages, which is due to the high

volumetric capacitance (C^*) of the channel material.[9] g_m is an important parameter that describes the signal amplification of a transistor. Transconductance indicates how much the change in input signals (V_G) can be converted to I_D and is defined using eqn (1) for OECTs:

$$g_m = \frac{\partial I_D}{\partial V_G} = \frac{Wd}{L}\mu C^*(|V_G - V_T|) \tag{1}$$

where W and L are the channel width and length, d is the channel thickness, μ is charge mobility, C^* is the volumetric capacitance of the channel, and V_T is the threshold voltage of the OECT.[10] Based on this equation, g_m depends on channel geometry (W, L, d) and the applied gate bias (V_G). The inherent material characteristics are the charge mobility μ, and the volumetric capacitance C^*. The product of these two values is utilized as a figure of merit (μC^*) for benchmarking the OECT channel materials.[11]

Organic semiconductors are capable of transporting electronic charges along their π-conjugated molecular structures both intra- and intermolecularly. The operation of OECTs relies on

[a] Department of Chemical and Materials Engineering, University of Alberta, Edmonton, Alberta, T6G 1H9, Canada

[b] Department of Electrical and Computer Engineering, University of Alberta, Edmonton, Alberta, T6G 1H9, Canada. E-mail: mgupta1@ualberta.ca

the interaction between the channel material and ions from the electrolyte to modulate current, indicating both ion and electron transports are essential. Researchers have introduced the term organic mixed ionic-electronic conductors (OMIECs) to distinguish this novel type of material.[12–14] Similar to organic semiconductors, OMIECs can be categorized into two types based on the charge carriers: p-type and n-type. Many p-type OMIECs have been reported and applied in applications due to their high performance and stability. However, electron-transporting n-type OMIECs have been far less studied than the p-type OMIECs. They have lower electron mobility and are relatively unstable under ambient conditions compared to their p-type counterparts.[15] Recently, significant progress has been made in developing n-type OMIECs, including the synthesis of materials *via* green chemistry, which demonstrates exceptional n-type performance and stability.[16,17] Developing highly stable and high-performance n-type OMIECs would enable the development of complementary circuit OECTs when coupled with p-type materials.

Poly(3,4-ethylenedioxythiophene) polystyrene sulfonate (PEDOT:PSS) is the most commonly used OMIEC for depletion mode OECTs, which exhibit an ON state without applied gate potential ($V_G = 0$). When a gate potential is applied to the OMIECs channel *via* the gate electrode, resulting in the depletion of charges by the injection of ions from the electrolyte, the channel conductivity and drain current (I_D) decrease. On the other hand, in accumulation mode OECTs, the device is in the OFF state when $V_G = 0$. When a gate bias is applied, OMIECs are doped by the ions from the electrolyte. This process leads to an increase in I_D, and the device turns ON. Therefore, OECTs operating in accumulation mode require less power than those in depletion mode.[2]

Solution processing techniques are widely used for OECT fabrication, offering several advantages, such as low-cost fabrication, room-temperature compatibility, scalability, and rapid processing. Spin-coating is one of the popular solution-processing methods for creating thin and uniform films. For this technique, an excess amount of organic semiconductor solution is dispensed onto the substrate, which is then rotated at a high speed to achieve a controlled film thickness. As spin-coating produces a continuous film covering the entire substrate, patterning is usually achieved through separate steps.[18] Drop-casting technique is another simple, rapid, and effective method for depositing OMIECs to the desired region, where a small volume of solution droplet is directly deposited onto the substrate, which forms a thin film upon solvent evaporation. While the solvent evaporates, OMIEC molecules are self-assembled by their intermolecular interactions. However, the coffee ring effect can result in inconsistent channel geometries and limit the reproducibility of this method.[19]

In our previous work, we have successfully synthesized naphthalene diimide (NDI)-based n-type small molecule OMIEC, gNDI-Br$_2$, and characterized its electrochemical behaviours, morphology, and microstructures. We also fabricated OECT devices utilizing gNDI-Br$_2$ through drop-casting and demonstrated its potential as an OECT active channel material.

The fabricated gNDI-Br$_2$ OECT operated as an n-type accumulation mode device and exhibited an excellent transconductance value of ~350 μS using a 50 mg mL^{-1} gNDI-Br$_2$ solution in chloroform (CHCl$_3$), and excellent cycling stability within 36 minutes of continuous pulsing and 22.3% decrease in I_D.[20] Since the gNDI-Br$_2$ is a new small-molecule OMIEC, and its capability as an OECT channel material was reported for the first time, gNDI-Br$_2$ fabrication processing parameters, such as solution concentration, film thickness, and annealing temperature, need to be examined.

Hence, these processing parameters were evaluated in this work. To investigate the effect of the solution concentration on drop-cast gNDI-Br$_2$ OECTs, different concentrations of gNDI-Br$_2$ in CHCl$_3$ were prepared and used in OECT fabrication. A range of concentrations (10, 20, 30, 40, 50, and 100 mg mL^{-1}) was examined to identify their effects on OECT g_m. OECT channel thickness is an important parameter which impacts g_m, but gNDI-Br$_2$ thin film presents a challenge in accurately measuring its thickness using tools due to its softness. The number of deposited gNDI-Br$_2$ layers was used instead of the actual thickness to investigate the effect of thickness on the OECT transconductance. Lastly, gNDI-Br$_2$ thin films were annealed at various temperatures. The thermal treatment is expected to promote thin film quality by facilitating the rearrangement of the gNDI-Br$_2$ molecules, resulting in enhanced OECT performance.

Experimental section

OECT Device fabrication

gNDI-Br$_2$ was synthesized using the method previously reported.[20] Different concentrations of gNDI-Br$_2$ solution (10, 20, 30, 40, 50, and 100 mg mL^{-1}) were prepared in CHCl$_3$. A volume of 0.2 μL of gNDI-Br$_2$ solution from each concentration was drop-cast onto the gold (Au) source/drain electrodes on Si/SiO$_2$ substrates as described in our work, and the average thickness of the film (50 mg mL^{-1}) was estimated as 1.21 μm.[20] The drop-casting is carefully controlled, resulting in an average film area of 7.85 $\pm$ 1.83 mm^2 ($n = 3$) when drop-casting 1-layer of 50 mg mL^{-1} gNDI-Br$_2$ solution. For the multi-layer gNDI-Br$_2$ OECTs, the same volume of 50 mg mL^{-1} gNDI-Br$_2$ solution was drop-cast onto the substrates up to ten times.

For the thermal treatment, a hot plate was used to anneal the drop-cast gNDI-Br$_2$ thin film. A 0.2 μL of 50 mg mL^{-1} gNDI-Br$_2$ solution was deposited onto the gold source/drain electrodes on Si/SiO$_2$ substrates, followed by 24-hour annealing at 40, 80, or 120 °C under ambient conditions. During annealing, the drop-cast gNDI-Br$_2$ OECT was covered with an aluminum foil-wrapped Petri dish to shield the device from potential disruptions.

Morphology and crystallinity characterization

Solutions of 50 mg mL^{-1} gNDI-Br$_2$ in CHCl$_3$ were drop-cast onto a silicon (100) wafer, followed by annealing at different temperatures (40, 80, and 120 °C) for 24 hours. The prepared

gNDI-Br$_2$ thin films were then imaged using a Zeiss EVO M10 SEM. XRD analyses were carried out on the same samples using a Rigaku XRD Ultima IV with a D/teX ultra detector. The results were obtained with the scan-axis 2 theta (2θ) ranging from 3° to 30° with a step size of 0.03°.

OECT characterization

A Keithley 2612b sourcemeter with customized LabView control software were used to measure OECT electrical characteristics. An Ag/AgCl wire was used as the gate electrode, and 100 mM NaCl solution was used as the electrolyte. The device output characteristics (I_D vs. V_D) were collected by measuring the drain current (I_D) while sweeping V_D from −0.1 to +0.8 V at various V_G with a step increment of 0.05 V. To ensure the devices operate within their stability window, different V_G ranges were used. For 1-layer drop-cast devices, a V_G range of 0–0.4 V was used. For devices with channel layers of 3, 5, 6, 7, and 8, they were characterized using a V_G range of 0–0.5 V. For 9- and 10-layer devices, a V_G range of 0–0.55 V was utilized. The transfer curves (I_D vs. V_G) were obtained for V_D = 0.8 V, and the corresponding g_m values were calculated from the slope of the transfer curve based on eqn (1). The averages of $I_{D,max}$ and $g_{m,max}$ were taken from three measurements on different devices. After each measurement, the OECT was rinsed with DI water to remove NaCl electrolyte residue and dried in a vacuum desiccator.

Results and discussion

Effect of concentrations of gNDI-Br$_2$

To evaluate the effect of gNDI-Br$_2$ solution concentrations on device performance, OECTs were prepared by drop-casting gNDI-Br$_2$ solutions of various concentrations (10, 20, 30, 40, 50, and 100 mg mL^{-1}) between Au source and drain electrodes with different channel lengths (10, 20, 50, 100 μm) on Si/SiO$_2$ substrate. The steady-state characteristics of the devices were measured as illustrated in Fig. 1(a). The processing parameter that resulted in the best performance was determined according to the peak transconductance ($g_{m,max}$) value. A typical drop-cast device is shown in Fig. 1(b), where only the region between the source and drain electrode was considered for the channel dimensions as illustrated in Fig. S1. Since the same solution volume was used when drop-casting for all devices, the actual channel length was entirely dependent on drop-casting location and solution wettability on the substrate, which may vary. Among all combinations tested, OECTs with 10 μm channel length using 100 mg mL^{-1} solution exhibited the best performance (Fig. 1(c) and (d)), achieving a $g_{m,max}$ of 862.7 μS. These devices operated in n-type accumulation mode, which was consistent for all concentrations and channel lengths, where I_D increases with V_G because of the Na$^+$ ions in the electrolyte coupling with the carbonyl oxygen on NDI, consistent with our previous findings.

Despite solution concentration change, OECTs with channel lengths of 10 and 20 μm demonstrated the most consistent performances (Fig. S2–S7), and their key device parameters are summarized in Table 1. For a fixed channel length, $I_{D,max}$ increases as the gNDI-Br$_2$ solution concentration increases from 10 mg mL^{-1} to 100 mg mL^{-1}. This behaviour is attributable to the increased number of gNDI-Br$_2$ molecules with the higher solution concentration, which leads to densely packed channel films and enhanced intermolecular charge transport within the channel, and hence increased channel conductivity. Similarly, g_m values increase as the gNDI-Br$_2$ solution increases (Fig. 1(e)–(f), Fig. S3, S6), indicating the performance of the OECT correlates well with the concentration of the gNDI-Br$_2$. For all functional devices, only small threshold voltages (V_T < 0.2 V) were needed to turn the OECT ON, indicating their low power consumption. In contrast, for devices fabricated using source and drain electrodes spaced at 50 and 100 μm, low yields were observed among all concentrations tested. Only one or two out of five fabricated devices were found to operate as compared to the 90–95% operational devices for 10 and 20 μm spacings. This performance limitation was only observed for devices with longer channel lengths and is likely attributed to the relatively short molecular length of gNDI-Br$_2$. Unlike polymeric OMIECs, gNDI-Br$_2$ is a small molecule material that may be challenging to span between wider S/D electrode spacings. The resulting channel films are more prone to defects and discontinuities, limiting their charge transport efficiency.

This can be further supported by the morphology study of drop-cast gNDI-Br$_2$ thin films at each concentration, which has been investigated in our previous work using SEM.[20] The gNDI-Br$_2$ molecules demonstrated a strong tendency to aggregate due to their molecular interactions, resulting in a morphology with agglomerates of gNDI-Br$_2$ molecules on the film surface. For the solution concentrations below 50 mg mL^{-1}, the amount of gNDI-Br$_2$ was insufficient to completely bridge the source and drain electrodes, resulting in small voids in the channel when drop-casting only one layer. The discontinuous channel film affects OECT performance consistency. Conversely, when the concentration reaches 50 mg mL^{-1}, the gNDI-Br$_2$ molecules fully cover the entire channel area without any gaps, resulting in functional and repeatable OECTs. This observation can be well correlated with the device properties shown in Table 1. For concentrations below 50 mg mL^{-1}, there was only a small increase in $I_{D,max}$ and $g_{m,max}$; a more substantial increase in these values was observed for higher gNDI-Br$_2$ concentrations (> 50 mg mL^{-1}). Since gNDI-Br$_2$ is a small molecule material with a lower molecular weight compared to other reported polymeric OMIECs, it is essential to have a continuous thin film where the molecules are densely packed for efficient charge transport to ensure OECT device performance. Based on the combined electrical and morphological analysis, the concentration of 50 mg mL^{-1} was selected to fabricate OECTs for the rest of this study to investigate additional processing parameters.

Effect of drop-cast gNDI-Br$_2$ layers

Volumetric doping of OMIECs, induced by ion insertion from the electrolytes during OECT operation, occurs throughout the entire bulk channel. Therefore, the thickness of the OMIECs
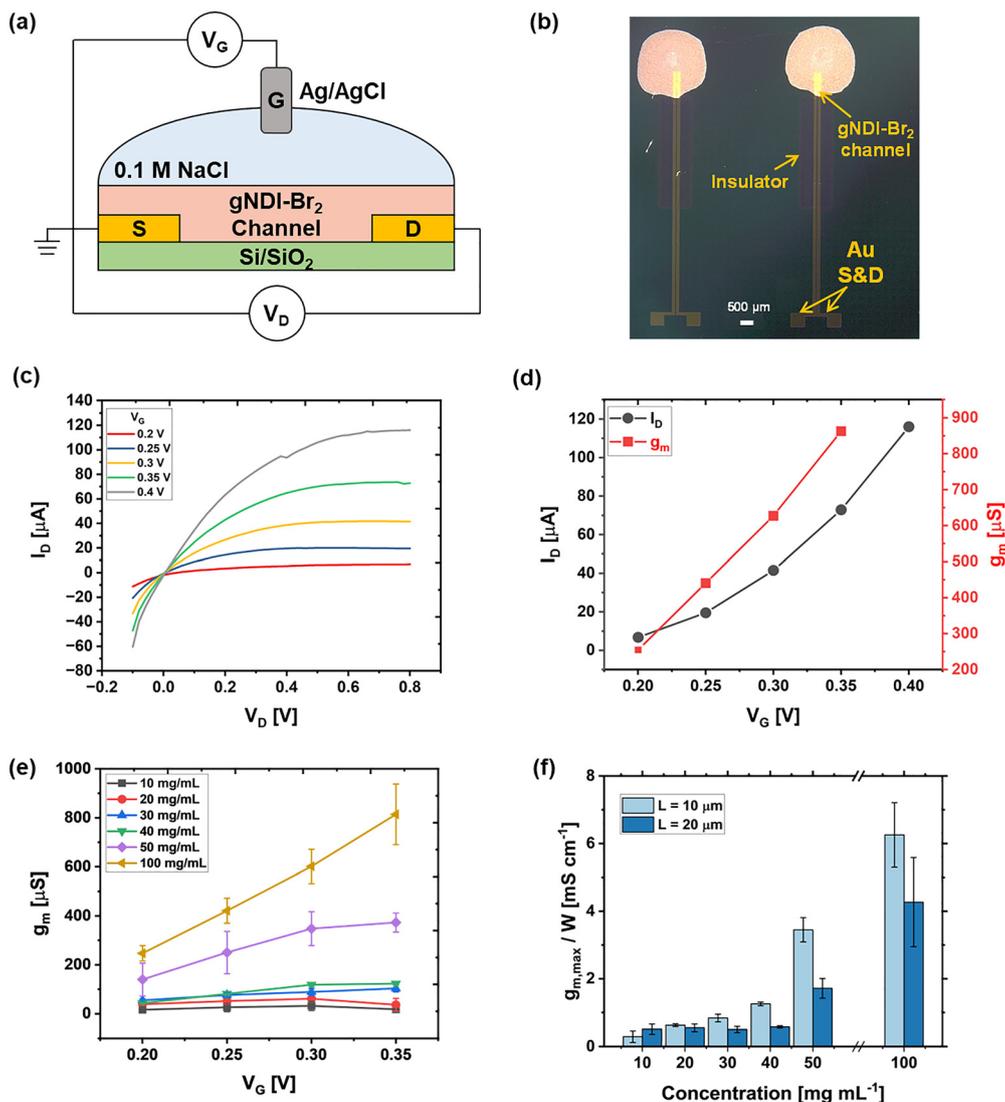
Fig. 1 (a) Side-view schematic of gNDI-Br$_2$ based n-type accumulation OECT. (b) Microscope image of gNDI-Br$_2$ (50 mg mL^{-1}) OECT with channel length (L) of 50 μm. (c) Steady-state output characteristics of a single-layer gNDI-Br$_2$ (100 mg mL^{-1}) OECT (L = 10 μm) measured with a 100 mM NaCl electrolyte and Ag/AgCl gate electrode. (d) Transfer and transconductance curves at V_D = 0.6 V for the same device. (e) Transconductance curves of OECTs (L = 10 μm) fabricated using different concentrations of gNDI-Br$_2$ solutions. (f) Average $g_{m,max}/W$ vs. gNDI-Br$_2$ concentration for devices with L = 10 and 20 μm.

channel is a crucial parameter influencing OECT device performance.[21,22] Based on eqn (1), the OECT transconductance is directly proportional to the channel thickness (d). However, due to the softness of gNDI-Br$_2$ thin films, direct measurement of their thickness using contact-based techniques is challenging. Hence, we utilized the number of deposited gNDI-Br$_2$ layers as a variable for controlling the final channel thickness. We drop-cast different numbers of 50 mg mL^{-1} gNDI-Br$_2$ layers onto microfabricated gold source/drain electrodes with L = 10 and L = 20 μm spacings on Si/SiO$_2$

Table 1 Summary of the average device geometry (W/L), the normalized maximum drain current ($I_{D,max}/W$), and normalized peak transconductance ($g_{m,max}/W$) for n-type OECTs fabricated with different concentrations of gNDI-Br$_2$ solutions by drop-casting one layer

Solution concentration		10 mg mL^{-1}	20 mg mL^{-1}	30 mg mL^{-1}	40 mg mL^{-1}	50 mg mL^{-1}	100 mg mL^{-1}
L = 10 μm	W/L	109.5	97.7	123.1	97.6	108.1	130.1
	$I_{D,max}/W$ (μA cm^{-1})	42.3 ± 32.1	92.3 ± 16.9	158.1 ± 6.6	199.2 ± 4.5	558.3 ± 142.2	866.8 ± 104.6
	$g_{m,max}/W$ (mS cm^{-1})	0.29 ± 0.17	0.63 ± 0.04	0.84 ± 0.11	1.26 ± 0.06	3.45 ± 0.36	6.25 ± 0.95
L = 20 μm	W/L	30.8	46.6	65.2	68.9	43.5	46.6
	$I_{D,max}/W$ (μA cm^{-1})	64.0 ± 16.9	68.6 ± 12.2	98.7 ± 33.6	110.2 ± 16.9	254.4 ± 45.7	610.8 ± 320.8
	$g_{m,max}/W$ (mS cm^{-1})	0.51 ± 0.15	0.55 ± 0.11	0.50 ± 0.09	0.57 ± 0.03	1.71 ± 0.29	4.26 ± 1.31

substrate and investigated their influences on the OECT's behaviours and properties. The key device parameters are listed in Table 2. Among all device configurations, OECTs with 10-layer gNDI-Br$_2$ channel and $L = 10$ μm exhibited the best performance as shown in their output and transfer characteristics (Fig. 2(a) and (b)), with a peak transconductance of 1350.7 μS.

Analysing the electrical characteristics of devices with $L = 10$ μm (Fig. S8–S10), we observed that as the number of deposited gNDI-Br$_2$ layers increases, the maximum I_D increases with a higher V_G allowed to be applied. For 1-layer gNDI-Br$_2$ OECT (Fig. S8(a)), a maximum I_D occurred at $V_G = 0.4$ V beyond which no further increase in I_D was observed. For the 3-, 5-, 6-, 7-, and 8-layer gNDI-Br$_2$ OECTs (Fig. S8(b)–(f)), the gNDI-Br$_2$ OECTs can tolerate up to V_G of 0.5 V, and the 9- and 10-layer OECTs (Fig. S8(g) and (h)) can withstand a V_G of 0.55 V. These results suggest that increasing the number of deposited gNDI-Br$_2$ layers leads to a thicker channel with more gNDI-Br$_2$ molecules; hence, a higher V_G is required to drive sufficient ions from the electrolyte to fully dope the channel to achieve maximum output current. Fig. 2(c) displays the transconductance curves of the multi-layer gNDI-Br$_2$ OECTs with $L = 10$ μm. As the number of deposited layers increases, a corresponding enhancement in the average $g_{m,max}$ was observed from 113.0 ± 19.6 μS for devices with a single-layer channel to 1138.4 ± 193.2 μS for those with a 10-layer channel, demonstrating a nearly 10-fold increase. This increase correlates directly with the channel thickness and aligns with eqn (1), as the total channel capacitance increases with thickness, a unique property observed for OMIEC-based devices. Similarly, a consistent increase in normalized $I_{D,max}$ was observed, ranging from 103.0 ± 25.1 μA cm^{-1} to 1128.4 ± 193.2 μA cm^{-1}. This indicates that an increased amount of the gNDI-Br$_2$ molecules in the OECT channel leads to proportionally higher electronic conductivity during OECT operation.

The average $g_{m,max}$ values for the two groups of devices are plotted against their channel layers as shown in Fig. 2(d). Devices with short channel length ($L = 20$ μm) demonstrated consistent increase in their gain values with the increasing number of layers. However, for devices with longer channel ($L = 20$ μm), there was no consistent device performance increase with the number of deposited channel layers (Fig. S11–S13). It is also worth noting that despite the channel dimensions, the gNDI-Br$_2$ exhibits an average V_T less than 0.2 V (Fig. S10 and S12), confirming their low-power operation. Based on these results, we confirm that gNDI-Br$_2$ exhibits volumetric doping, suggesting that gNDI-Br$_2$ is a functional material as OECT active channels.

Effect of thermal annealing

Another processing parameter we assessed is the annealing temperature for gNDI-Br$_2$ thin films during fabrication. Thermal annealing is known to influence the molecular packing and film morphology in solution-processed techniques by enhancing solvent evaporation rates and molecular mobility. We prepared gNDI-Br$_2$ thin films on silicon (Si) wafers for thin

Table 2 Summary of the device geometry (W/L), the normalized maximum drain current ($I_{D,max}/W$), and normalized peak transconductance ($g_{m,max}/W$) for n-type gNDI-Br$_2$ (50 mg mL^{-1}) OECTs fabricated via drop-casting with different numbers of gNDI-Br$_2$ layers

| Channel layers		1 layer	3 layers	5 layers	6 layers	7 layers	8 layers	9 layers	10 layers
$L = 10$ μm	W/L	121.5	270.9	236.3	373.2	251.4	182.3	295.5	302.8
	$I_{D,max}/W$ [μA cm^{-1}]	103.0 ± 25.1	130.2 ± 35.0	297.3 ± 42.9	198.1 ± 44.5	341.4 ± 70.4	470.7 ± 176.0	646.0 ± 208.5	1018.2 ± 254.6
	$g_{m,max}/W$ [mS cm^{-1}]	0.93 ± 0.16	0.56 ± 0.02	1.26 ± 0.12	0.97 ± 0.08	1.63 ± 0.03	2.38 ± 0.28	2.64 ± 0.11	3.73 ± 0.64
$L = 20$ μm	W/L	32.0	101.2	111.9	113.8	135.1	132.1	136.3	126.5
	$I_{D,max}/W$ [μA cm^{-1}]	70.4 ± 5.2	63.5 ± 10.5	163.4 ± 47.9	202.4 ± 28.5	214.4 ± 77.1	209.2 ± 55.7	253.3 ± 73.6	276.0 ± 94.2
	$g_{m,max}/W$ [mS cm^{-1}]	0.44 ± 0.06	0.28 ± 0.02	0.65 ± 0.05	0.77 ± 0.04	0.66 ± 0.08	0.72 ± 0.17	0.75 ± 0.13	0.97 ± 0.09
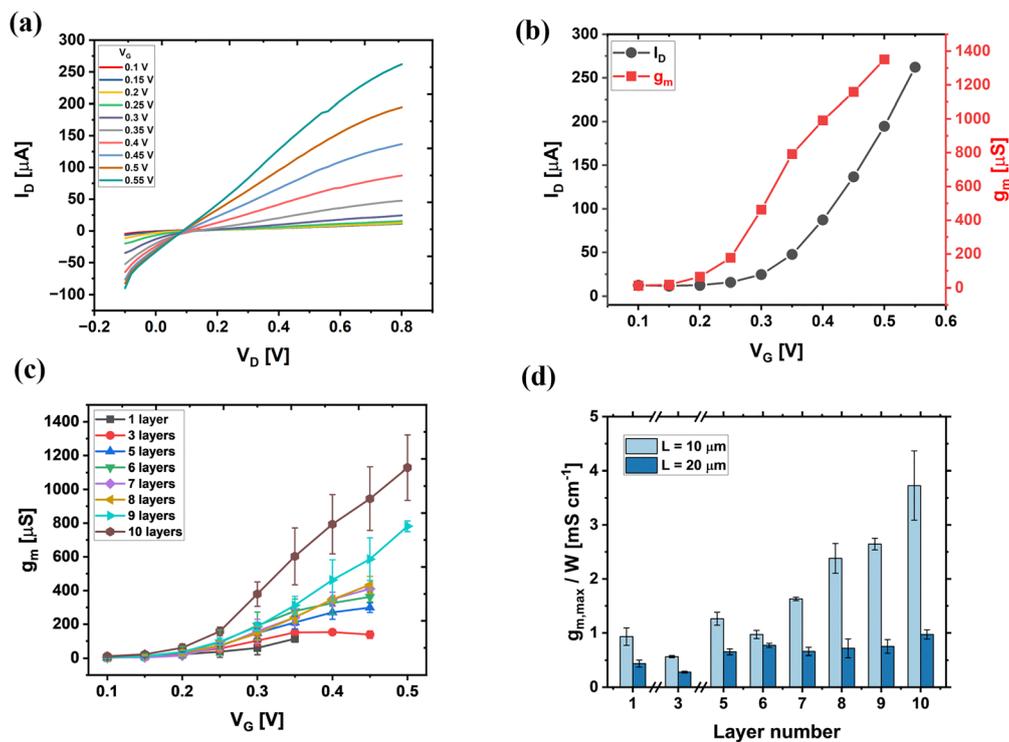
Fig. 2 (a) Output characteristics of 10-layer drop-cast gNDI-Br$_2$ OECTs (50 mg mL^{-1}) with L = 10 μm. (b) The corresponding transfer and transconductance curves for the same device 10 layer device. (c) Transconductance curve comparison of OECTs with different numbers of drop-cast layers and L of 10 μm. (d) Average $g_{m,max}$ vs. number of drop-cast channel layers for devices with L = 10 μm and 20 μm. Error bars are the standard deviation with n = 3. All measurements were performed using 100 mM NaCl electrolyte and Ag/AgCl wire as the gate electrode.

film characterization and fabricated OECT on Si/SiO$_2$ substrates with gold source/drain electrodes with L = 10 μm. Immediately after drop-casting the gNDI-Br$_2$ solution onto the substrates, the thin films were heated on a hot plate.

Fig. 3(a) presents the X-ray diffraction (XRD) results of gNDI-Br$_2$ thin films annealed at different temperatures. In contrast to our previous gNDI-Br$_2$ GIWAXS report,[20] which showed multiple packing motifs, only the brick-wall packing was observed from the XRD spectra in this study. For the gNDI-Br$_2$ thin film

annealed at 40 °C, a single peak appeared at the 2 thetas (2θ) of 3.81°, corresponding to a d-spacing calculated of 23.17 Å. This value is in close agreement with the intermolecular distance q_z = 0.262 Å^{-1} (d = 23.98 Å), as derived from the previous GIWAXS results.[20] Upon increasing the annealing temperature to 80 °C, three peaks emerged at 2θ = 3.27° (d = 26.99 Å), 3.87° (d = 22.81 Å), and 6.33° (d = 13.95 Å), respectively. These peaks indicate molecular structural rearrangement of the film, which is likely associated with straightening of the linear glycol side
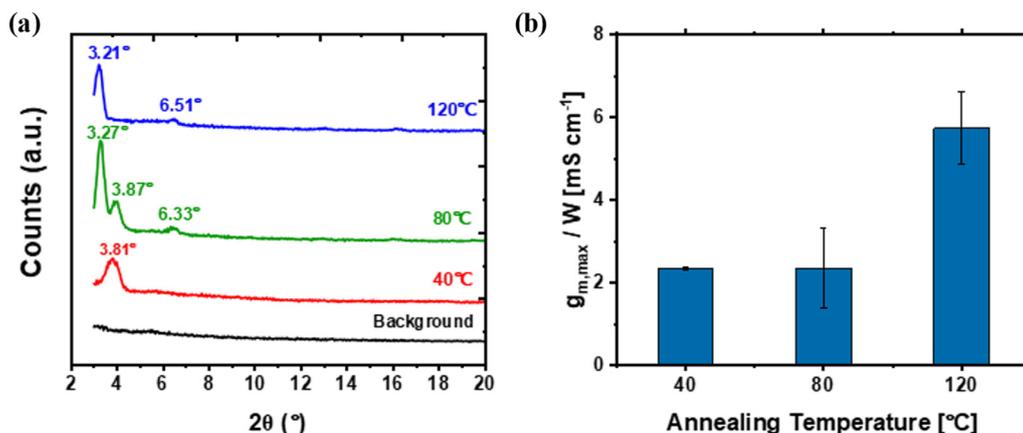

Fig. 3 (a) X-ray diffraction (XRD) patterns and (b) average normalized $g_{m,max}$ vs. annealing temperature of the thermal-treated gNDI-Br$_2$ thin film (50 mg mL^{-1}, 1-layer) annealed at 40 °C, 80 °C, and 120 °C under ambient conditions.

Table 3 Summary of the geometry (W/L), the maximum drain current ($I_{D,max}$), and normalized peak transconductance ($g_{m,max}/W$) for drop-cast gNDI-Br$_2$ (50 mg mL^{-1}, 1-layer) OECTs fabricated onto Si/SiO$_2$ substrate with different annealing conditions (40 °C, 80 °C, and 120 °C)

Annealing temperature	Without annealing	40 °C	80 °C	120 °C
W/L	121.5	79.7	68.0	58.4
$I_{D,max}$ [µA]	12.5	37.4	35.5	46.4
$g_{m,max}/W$ [mS cm^{-1}]	0.93 ± 0.16	2.33 ± 0.04	2.34 ± 0.97	5.73 ± 0.87

chains and resulted in an increased d-spacing compared to the thin film annealed at 40 °C. The shift of the primary peak from 3.87° to 3.81°, along with the emergence of the new peak at 3.27°, indicated the coexistence of different d-spacings during the transition, suggesting that gNDI-Br$_2$ molecules were still in the process of rearrangement. A new peak appeared at 2θ = 6.33° (d = 13.95 Å) after annealing at 80 °C, which is likely attributed to a higher-order lamellar reflection. The gNDI-Br$_2$ thin film annealed at 120 °C exhibited two peaks in its XRD results, with 2θ values of 3.21° (d = 27.50 Å) and 6.51° (d = 13.57 Å), which are in similar 2θ regions compared to the sample annealed at 80 °C. These can be interpreted as brick-wall motif lamellar-like scattering and a possible higher-order lamellar peak, respectively. Additionally, the disappearance of the peak near 3.8° after annealing at 120 °C further indicates a more stable packing state for the film. It should be noted that in these XRD patterns, it is challenging to observe out-of-plane scattering peaks for the π–π spacing between gNDI-Br$_2$ molecules, likely due to the low intensity and high signal noise.

We further investigated the morphology of annealed gNDI-Br$_2$ thin film using scanning electron microscopy (SEM), and the results are illustrated in Fig. S14. In this case, annealing led to the formation of more densely aggregated microstructures of gNDI-Br$_2$, as expected due to improved molecular ordering under heat. This observation is consistent with our XRD results. However, when the annealing temperature was increased to 120 °C, visible cracks appeared on the gNDI-Br$_2$ thin films. The rapid rearrangement of gNDI-Br$_2$ molecules at high temperature disrupted the film uniformity due to thermally induced strain and insufficient cohesive interaction between the gNDI-Br$_2$ molecules and the substrate.

As observed from the output characteristics of annealed gNDI-Br$_2$ OECTs Fig. S15, there are noticeable differences for the OECT annealed at 120 °C, which demonstrates a saturation voltage ($V_{D,SAT}$) of approximately 0.25 V for V_G = 0.4 V. For the OECTs annealed at 40 °C and 80 °C (Fig. S15 (a) and (b)), determining the saturation voltage is challenging. This observation may be attributed to the smaller W/L for the device anneal at 120 °C, which also led to a lower V_T (Fig. S16). Furthermore, the device geometry (W/L), $I_{D,max}$, and $g_{m,max}/W$ results from the annealed gNDI-Br$_2$ OECTs are summarized in Table 3. There is a slight increment in the $I_{D,max}$ as the annealing temperature rises. The $I_{D,max}$ of the gNDI-Br$_2$ OECT annealed at 120 °C is 46.4 µA, even when the applied external gate potential is 0.45 V, whereas the others show 37.4 and

35.5 µA of $I_{D,max}$ at V_G of 0.5 V. $g_{m,max}$ also increased with the applied annealing temperature. The normalized transconductance comparison from each of the annealed gNDI-Br$_2$ OECTs is shown in Fig. 3(b). The highest $g_{m,max}/W$ was achieved for devices annealed at 120 °C (Table 3) with a substantial increase to 5.73 ± 0.87 mS cm^{-1}, which is a more than 5-fold increase compared to the sample without annealing and the most effective performance enhancement found in this study. Despite exhibiting the best device performance, fine cracks were observed for the NDI-Br$_2$ thin film annealed at 120 °C due to thermal stress. The cracks in the channel have led to device performance deterioration upon repeated measurements, with more than 10-fold $g_{m,max}$ reduction from 377.5 µS for the first measurement to only 31.7 µS for the 6th measurement (Fig. S17). Compared to devices without annealing, the OECT performance has improved by approximately 2.5-fold in their $g_{m,max}/W$ values after thermal treatment at 40 and 80 °C, which is consistent with the thermally triggered molecular rearrangement observed from XRD spectra. Thus, these results suggest that thermal annealing is an effective approach to enhance OECT performance.

The performance of drop-cast small-molecule OMIEC gNDI-Br$_2$ OECTs is highly dependent on key processing parameters, including solution concentration, layer number, and thermal treatment. The optimized devices exhibited a high normalized transconductance of 6.25 ± 0.95 mS cm^{-1}. When benchmarking this against other studies in the field, the performance of the gNDI-Br$_2$ OECTs is favorable for a device fabricated via simple drop-casting method. To the best of our knowledge, this is the only study for NDI-based small-molecule OECTs. The majority of NDI-based OMINCs reported in the literature are polymeric. For comparison, NDI-polymer OECTs, which are derived from gNDI-Br$_2$ as their pre-polymerization NDI comonomer precursor, typically exhibit similar device performances, such as g_m/W = 2.17 mS cm^{-1} for p(gNDI-gT2),[23] g_m/W = 0.19 S cm^{-1} for p(C3-gNDI-gT2),[24] and g_m/W = 1.13 S cm^{-1} for p(C$_4$-T2),[25] all with channel length of 10 µm. By further optimizing the molecular structure, crystallinity, and ion transport, the performance of n-type small-molecule based OECTs has been significantly improved in more recent studies. For example, the normalized g_m can reach 0.4 S cm^{-1} for fused small-molecule semiconductors,[26] and a high normalized g_m of 1.40 ± 0.13 S cm^{-1} has been reported for small-molecule gNR derivatives.[27] While in these studies, the superior performance is often achieved by molecular design, our results demonstrate the effectiveness of processing parameters for gNDI-Br$_2$ based OECTs. It should be noted that the use of drop-casting, although simple and effective, has significant limitations to the controllability and repeatability of channel dimensions, including area and thickness. Therefore, future efforts will focus on solution process techniques, such as printing, to achieve more precise dimensional control, which may further enhance device performance. The preliminary stability test demonstrated I_D maintained around 95% after 13 minutes of pulsed V_G measurement for gNDI-Br$_2$ OECTs.[20] Comprehensive investigations into operational stability and device shelf life will

be conducted in the future to ensure the reliability of the devices for practical applications. In addition, the small molecule gNDI-Br$_2$ can be used for other applications in photovoltaics, fuel cells, electrochromic devices. Hence, the material developed can have applications in a variety of areas and has the versatility of being fabricated *via* different techniques as it is solution processable.

Conclusions

In this study, we have explored the parameters affecting the performance of drop-cast gNDI-Br$_2$ OECTs. Each processing parameter, including solution concentration, device geometry, number of deposited gNDI-Br$_2$ layers, and thermal treatment, plays a significant role in device performance. We initially investigated the impact of different gNDI-Br$_2$ solution concentrations on OECT performance following thin film formation by drop-casting. Higher gNDI-Br$_2$ concentrations resulted in an increased number of gNDI-Br$_2$ molecules being deposited on substrates, which consequently enhanced OECT performance ($g_{m,max}/W$ = 6.25 $\pm$ 0.95 mS cm^{-1} for 100 mg mL^{-1}). Film thickness is another essential factor that affects OECT transconductance, but accurately measuring the thickness of gNDI-Br$_2$ thin films was challenging due to their softness. To evaluate the impact of channel thickness on OECT g_m, we introduced the concept of the number of deposited gNDI-Br$_2$ layers. As the deposited gNDI-Br$_2$ layers increased, the performance of gNDI-Br$_2$ significantly improved ($g_{m,max}/W$ = 3.73 $\pm$ 0.64 mS cm^{-1} for 10-layer). This enhancement can be attributed to the increased number of gNDI-Br$_2$ molecules and the subsequent increase in thickness. Finally, we tested thermal treatment and assessed its influence on thin film morphology, molecular arrangement, and OECT performance. The gNDI-Br$_2$ thin film annealed at higher temperatures demonstrated a more aggregated microstructure in the morphology. We investigated the molecular rearrangements during thermal treatment using XRD. These rearrangements corroborate the enhanced $g_{m,max}/W$ (5.73 $\pm$ 0.87 mS cm^{-1}) of the gNDI-Br$_2$ OECTs annealed at 120 °C. Although the OECT performance comparison is challenging due to the variation in device geometries of gNDI-Br$_2$ OECT fabricated by drop-casting, we have gained valuable insights that will guide the design and optimization of gNDI-Br$_2$ OECTs. Future work will focus on identifying different substrates to offer better adhesion and exploring fabrication techniques that allow fine-tuning of device geometry and performance for specific applications.

Author contributions

M. G. conceptualized and supervised the research project. S. K. carried out the most experiments and data analysis. J. F. assisted in OECT measurements and their analysis. S. K. wrote the original manuscript. All authors contributed to the manuscript editing and revision.

Conflicts of interest

There are no conflicts of interest to declare.

Data availability

The data supporting this article have been included as part of the supplementary information (SI). Supplementary information is available. See DOI: https://doi.org/10.1039/d5ma01045d.

More information can be obtained by contacting the corresponding author.

Acknowledgements

References

1 H. S. White, G. P. Kittlesen and M. S. Wrighton, *J. Am. Chem. Soc.*, 1984, **106**, 5375–5377.

2 J. Rivnay, S. Inal, A. Salleo, R. M. Owens, M. Berggren and G. G. Malliaras, *Nat. Rev. Mater.*, 2018, **3**, 17086.

3 W. Huang, J. Chen, Y. Yao, D. Zheng, X. Ji, L.-W. Feng, D. Moore, N. R. Glavin, M. Xie and Y. Chen, *Nature*, 2023, **613**, 496–502.

4 J. Y. Gerasimov, R. Gabrielsson, R. Forchheimer, E. Stavrinidou, D. T. Simon, M. Berggren and S. Fabiano, *Adv. Sci.*, 2019, **6**, 1801339.

5 P. C. Harikesh, D. Tu and S. Fabiano, *Nat. Electron.*, 2024, **7**, 525–536.

6 A. Marks, S. Griggs, N. Gasparini and M. Moser, *Adv. Mater. Interfaces*, 2022, **9**, 2102039.

7 I. Gualandi, M. Marzocchi, A. Achilli, D. Cavedale, A. Bonfiglio and B. Fraboni, *Sci. Rep.*, 2016, **6**, 33637.

8 P. R. Paudel, V. Kaphle, D. Dahal, R. K. Radha Krishnan and B. Lüssem, *Adv. Funct. Mater.*, 2021, **31**, 2004939.

9 D. Khodagholy, J. Rivnay, M. Sessolo, M. Gurfinkel, P. Leleux, L. H. Jimison, E. Stavrinidou, T. Herve, S. Sanaur, R. M. Owens and G. G. Malliaras, *Nat. Commun.*, 2013, **4**, 2133.

10 J. T. Friedlein, R. R. McLeod and J. Rivnay, *Org. Electron.*, 2018, **63**, 398–414.

11 S. Inal, G. G. Malliaras and J. Rivnay, *Nat. Commun.*, 2017, **8**, 1767.

12 A. Malti, J. Edberg, H. Granberg, Z. U. Khan, J. W. Andreasen, X. Liu, D. Zhao, H. Zhang, Y. Yao and J. W. Brill, *Adv. Sci.*, 2016, **3**, 1500305.

13 J. Rivnay, S. Inal, B. A. Collins, M. Sessolo, E. Stavrinidou, X. Strakosas, C. Tassone, D. M. Delongchamp and G. G. Malliaras, *Nat. Commun.*, 2016, 7, 11287.

14 Y. Wang, S. Wustoni, J. Surgailis, Y. Zhong, A. Koklu and S. Inal, *Nat. Rev. Mater.*, 2024, **9**, 249–265.

15 E. Zeglio and O. Inganas, *Adv. Mater.*, 2018, **30**, e1800941.

16 Y. Wang, A. Koklu, Y. Zhong, T. Chang, K. Guo, C. Zhao, T. C. H. Castillo, Z. Bu, C. Xiao and W. Yue, *Adv. Funct. Mater.*, 2024, **34**, 2304103.

17 Y. Wang, E. Zeglio, L. Wang, S. Cong, G. Zhu, H. Liao, J. Duan, Y. Zhou, Z. Li and D. Mawad, *Adv. Funct. Mater.*, 2022, **32**, 2111439.

18 B. R. Sankapal, A. Ennaoui, R. B. Gupta and C. D. Lokhande, *Simple Chemical Methods for Thin Film Deposition, Synthesis and Applications*, Springer, 2023, DOI: 10.1007/978-981-99-0961-2_1.

19 A. K. S. Kumar, Y. Zhang, D. Li and R. G. Compton, *Electrochem. Commun.*, 2020, **121**, 106867.

20 S. Kang, J. Fan, J. B. Soares and M. Gupta, *RSC Adv.*, 2023, **13**, 5096–5106.

21 S. S. Rezaie, D. Gudi, J. Fan and M. Gupta, *ECS J. Solid State Sci. Technol.*, 2020, **9**, 081003.

22 J. Rivnay, P. Leleux, M. Ferro, M. Sessolo, A. Williamson, D. A. Koutsouras, D. Khodagholy, M. Ramuz, X. Strakosas, R. M. Owens, C. Benar, J. M. Badier, C. Bernard and G. G. Malliaras, *Sci. Adv.*, 2015, **1**, e1400251.

23 A. Giovannitti, C. B. Nielsen, D. T. Sbircea, S. Inal, M. Donahue, M. R. Niazi, D. A. Hanifi, A. Amassian, G. G. Malliaras, J. Rivnay and I. McCulloch, *Nat. Commun.*, 2016, **7**, 13066.

24 I. P. Maria, B. D. Paulsen, A. Savva, D. Ohayon, R. Wu, R. Hallani, A. Basu, W. Du, T. D. Anthopoulos and S. Inal, *Adv. Funct. Mater.*, 2021, **31**, 2008718.

25 D. Ohayon, A. Savva, W. Du, B. D. Paulsen, I. Uguz, R. S. Ashraf, J. Rivnay, I. McCulloch and S. Inal, *ACS Appl. Mater. Interfaces*, 2021, **13**, 4253–4266.

26 J. Duan, G. Zhu, L. Wang, J. Chen, S. Cong, X. Zhu, Y. Zhou, Z. Li, I. McCulloch and W. Yue, *Adv. Funct. Mater.*, 2022, **32**, 2203937.

27 X. Zhu, J. Chen, R. Liu, C. Chen, J. Tan, C. Ran, Y. Wang, R. Wang, Z. Li and W. Yue, *J. Mater. Chem. C*, 2025, **13**, 1784–1792.